Importance of being cross-linked for the bacterial cell wall

Garima Rani[1,2] and Issan Patri[3]
[1]*Institute of Mathematical Sciences, C I T Campus, Chennai 600 113, India*
[2]*Homi Bhabha National Institute, Training School Complex, Anushakti Nagar, Mumbai 400094, India*
[3]*Chennai Mathematical Institute, SIPCOT IT Park, Siruseri, Chennai 603103, India*

(Received 30 April 2019; published 16 December 2019)

The bacterial cell wall is primarily composed of a mesh of glycan strands cross-linked by peptide bridges and is essential for safeguarding the cell. The structure of the cell wall has to be stiff enough to bear the high turgor pressure and sufficiently tough to ensure protection against failure. Here we explore the role of various design features of the cell in enhancing the toughness of the cell wall. We explain how the glycan strand length distribution, the degree of cross-linking and the placement of the cross-links on the glycan strands can act in tandem to ensure that the cell wall offers sufficient resistance to propagation of cracks. Further, we suggest a possible mechanism by which peptide bond hydrolysis, via judicious cleaving of peptide cross-links, can act to mitigate this risk of failure. We also study the reinforcing effect of MreB cytoskeleton, which can offer a degree of safety to the cell wall. However, we show that the cross-linked structure of the cell wall is its primary line of defense against mechanical failure.

DOI: 10.1103/PhysRevE.100.062408

I. INTRODUCTION

Understanding the design features of bacterial cells has long been a fundamental topic of research and a key design feature of bacteria is the cell wall. The bacterial cell wall is primarily composed of a sturdy mesh of glycan strands, consisting of chain of alternating amino sugars N-acetylglucosamine (NAG) and N-acetylmuramic acid (NAM), cross-linked by peptide bonds, known as the peptidoglycan network. The cell wall plays multiple roles, including protecting the cell against external threats and providing the cell its characteristic shape [1–4]. It has traditionally been an important target of antibiotics like penicillin and its derivatives. However, as several strains of bacteria are becoming resistant to antibiotics [5,6], understanding the structure of the bacterial cell wall assumes renewed significance, so that newer antibacterial agents that target the cell wall can be designed.

Toughness, or resistance to propagation of cracks, is an immensely desirable materials property [7]. A common problem encountered when materials are engineered is to ensure not only strength, specifically stiffness, but also toughness, which can be difficult as these two requirements are often at odds [8]. Biological materials in particular have to be structurally strong enough to resist high tension forces and sufficiently tough to prevent failure due to cracking. Indeed, several biological materials like wood, bones, and nacre serve as some of the best examples satisfying this requirement, with their specific design principles being well studied in this context [9–11]. For the bacterial cell wall, it is imperative to be stiff enough to bear the high turgor pressure and maintain shape as well as being adequately tough. While the stiffness of the bacterial cell wall has been well studied [12–15], our aim here is to understand its toughness. The cell wall, which is under high turgor pressure, can have cracks on its surface as a consequence of its design [16], and these can play an important role in ensuring passage of nutrients and waste products through the peptidoglycan layer. In fact, permeability of cell walls of bacteria has been much studied [17–19], and pores of size as large as 10 nm in diameter have also been observed [20]. On the other hand, in bacteria like *Staphylococcus aureus*, mechanical crack propagation has been shown to drive daughter cell separation [21], which indicates that bacterial cells are adapted to be able to tune mechanical failure modes. However, the relation of the molecular level architecture of the cell wall to its toughness remained to be elucidated.

In this paper, we study the role of various design components of the cell in securing the cell wall by ensuring sufficient resistance to propagation of cracks. In particular, we examine the role of the geometry of the cell, the cross-linked polymeric structure of the cell wall and the role of the MreB cytoskeleton [22,23] in ensuring stabilization of the cell wall against crack propagation. Our model, specifically, studies the Gram-negative rod-shaped bacteria (e.g., *Escherichia coli*), with a single layer of the peptidoglycan mesh. In short timescales relevant to the problem, the behavior of the cell wall is perfectly elastic [24,25]. The peptidoglycan mesh in this case consists of glycan strands oriented on an average in the circumferential direction, cross-linked intermittently by peptide bonds [26]. Modelling the cell both as an elastic plate and cylindrical shell, we estimate the critical crack lengths under stress due to turgor pressure. We show that cross-linking is crucial for maintaining the integrity of the cell wall, since the minimum energy needed for crack propagation, called the tearing energy, is largely controlled by the degree of cross-linking. We exhibit the important role that appropriately cross-linked shorter length glycan strands can play in enhancing the tearing energy, which gives an explanation of striking experimental observations on the extensive presence of short length glycan strands in the peptidoglycan mesh [27] and the

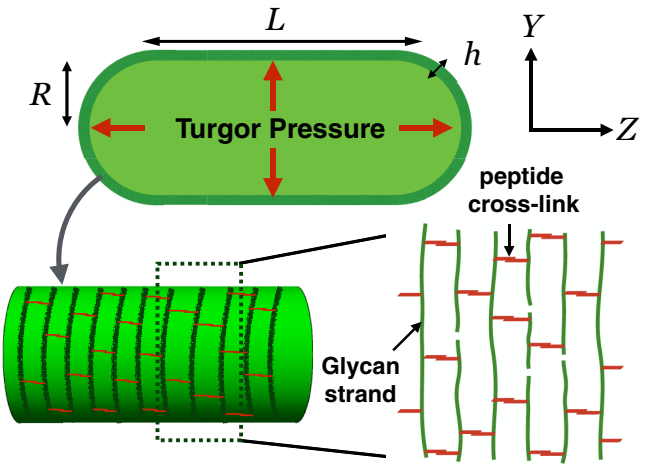

FIG. 1. The bacterial cell wall modeled as a pressurised cylindrical shell of radius R, thickness h and with the length denoted L. Glycan strands of variable lengths, aligned on an average in the circumferential direction, are cross-linked intermittently by peptide bonds.

strong propensity of the glycan strands to be cross-linked at the terminating units [28,29]. Our analysis suggests that peptide bond hydrolysis can be used by the cell as a defense mechanism against cracking, since such hydrolysis can act to increase the tearing energy. Finally, we probe the role of the MreB cytoskeleton which can promote cell wall toughness by exerting an inward directed pressure countering the turgor pressure. Our results indicate that the cross-linked structure of the cell wall plays the more important role in safeguarding the cell against failure due to crack propagation.

II. CELL WALL MODEL

We model the cell wall as a pressurized, linear elastic, thin cylindrical shell, as depicted in Fig. 1. We assume for simplicity that the shell is isotropic with elastic modulus denoted E. One can consider an orthotropic cell wall model [26] by modifying the strain energy release term (see Sec. III) for which additional elastic constants are required (as detailed in Appendix B). The radius of the shell is R and its thickness h. Since h/R is small (relevant parameter values are listed in Table I), we can treat the cell wall as effectively two dimensional, describing it by its central (neutral) surface. We use the thin shell "membrane" approximation, neglecting all moment expressions [34]. The turgor pressure is denoted P. Using force balance, the hoop stress is

$$\sigma_\phi = \frac{PR}{h}, \tag{1}$$

while the axial stress is

$$\sigma_z = \frac{PR}{2h}. \tag{2}$$

Hence a stress anisotropy exists in the cylindrical case, with $\sigma_\phi/\sigma_z = 2$.

TABLE I. Parameter values for *E. coli*.

Parameters	Values	References
Cell wall parameters:		
Radius of cell (R)	$\sim$0.5 μm	[30]
Thickness of the cell wall (h)	$\sim$5 nm	[31]
Turgor pressure (P)	1 atm	[24]
Elastic modulus of cell wall (E)	30 MPa	[13]
Glycan interstrand spacing (d)	2 nm	[26]
MreB parameters:		
Number of MreB molecules/cell (N)	17 000–40 000	[32]
Elastic modulus of MreB (E_{MreB})	(similar to actin)	[33]
	2 GPa	
MreB monomer diameter ($2r_0$)	5.1 nm	[22]

III. CELL WALL CRACK ENERGETICS

Since stress in the hoop direction is twice the stress in the axial direction, longitudinal cracks are subject to a larger stress, as they are aligned perpendicular to the hoop direction. Indeed, cylindrical pressure vessels predominantly display longitudinal cracks, for this reason, including well-known examples occurring in daily life like sausages and pipes cracking longitudinally [35]. For rod-shaped bacteria, like *E. coli*, which is under high turgor pressure, a corresponding stress anisotropy indicates the possibility of similar failure due to cracking in the longitudinal direction. Our aim here is to understand the structural features of the cell wall which protect it from such failure along the axial direction. We model a crack on the cell wall in two ways: (1) by considering a centrally placed crack on an infinite plate, thus neglecting curvature effects and (2) considering a longitudinally aligned crack on a pressurized shell, thus accounting for cell curvature.

In the first case, we begin with a thin plate of thickness h placed in the YZ plane, with a tensile load $\sigma = PR/h$ applied in the Y direction. A crack of total length $2c$ is introduced, along the Z axis, as shown in Fig. 2(a). The crack lengths of interest to us are considerably smaller than the radius and length of the cell wall. We can thus treat the plate as infinite. To calculate the critical crack length, beyond which crack propagation becomes energetically favorable, we use an energy balance criterion, pioneered by Griffith [36] which compares the energy required to break atomic bonds, thus leading to new surfaces, to the strain energy released as the crack enlarges (assuming that no energy dissipation occurs). The strain energy released in this case is given by

$$\mathcal{E}_p = \frac{\sigma^2}{E} h\pi c^2. \tag{3}$$

In the case of an orthotropic model of the cell wall, this term has to be modified with additional elastic constants incorporated into the expression (in Appendix B, we show that under reasonable assumptions, the strain energy released in the anisotropic model is comparable to the isotropic model used here).

The critical crack length is given by

$$c_f = \frac{G_0 E h^2}{\pi P^2 R^2}, \tag{4}$$

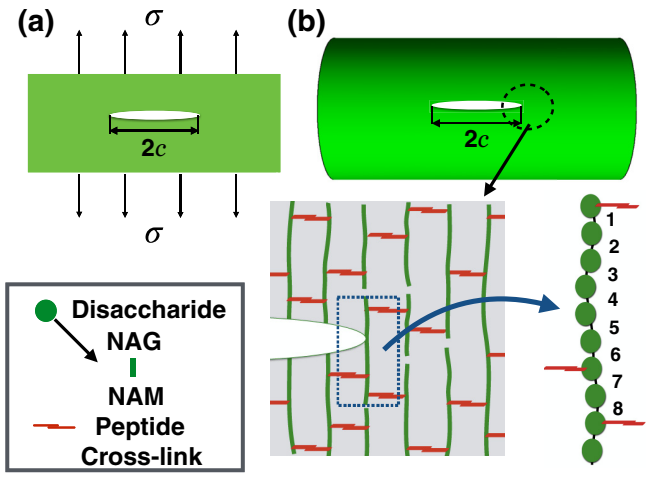

FIG. 2. (a) A crack of length $2c$ on a thin plate of thickness h with a remote load σ acting on it, perpendicular to the line of crack. (b) A longitudinally aligned crack on the cell wall. Near the tip, the crack comes up against a glycan strand, here illustrated having a length of 10 disaccharide units, with average number of glycosidic bonds connecting the disaccharides between adjacent cross-links calculated as $n = 4$. Each disaccharide unit consists of alternating sugars NAG and NAM connected by a glycosidic bond. Note that the depiction of the peptidoglycan sacculus here is illustrative, in general, the meshwork might exhibit high amount of disorder.

where G_0 denotes the minimum tearing energy (see Appendix A). We note that this paradigm of modeling curved objects by flat surfaces has been utilized widely, in the case of both bacteria [37] and other cells [38].

In the second case, we incorporate the cell curvature into our calculation. We consider a longitudinally aligned crack of length $2c$ on a thin, pressurized, cylindrical shell as shown in Fig. 2(b). In this case, the effect of geometry and the internal pressure results in an out-of-plane deformation of the shell in the periphery of the crack, due to which an additional strain energy is released, as compared to crack on a plate [39–41]. The total strain energy released in this case is

$$\mathcal{E}_i \simeq \mathcal{E}_p\left(1 + \frac{c^2}{Rh}\right) \tag{5}$$

(see Appendix C for more details). We can now calculate the critical crack length c_f using energy balance criterion, as the unique (positive) real root of the cubic equation

$$2c^3 + cRh - \frac{G_0 E R h}{\pi \sigma^2} = 0, \tag{6}$$

where $\sigma = \sigma_\phi = PR/h$.

To understand the effect of geometry of the cell wall, a comparison of these two cases needs to made. For this, we first need to compute the minimum tearing energy G_0, which we do in the following section.

A. Tearing energy: Role of cross links

A crack typically propagates by rupturing the bonds lying across its plane [42]. The tearing energy is conventionally calculated by estimating the energy cost for disrupting the bonds lying across the plane of the crack. However, in a cross-linked polymer, as the crack propagates, it encounters chains of monomers lying between adjacent cross-links. The forces involved are transmitted through the cross-links. So, in order to break the chain, each bond in the chain has to be supplied energy almost equaling the energy required to rupture them even though one of the bonds might eventually rupture [43,44]. Thus, the cross-linked polymeric structure of the peptidoglycan mesh can safeguard the cell against mechanical failure by resisting crack propagation in this manner.

For an axially aligned crack on the cell wall to propagate, it must cross a number of glycan strands cross-linked by peptide bridges. Glycan strands are made up of repeating disaccharide units of N-acetylglucosamine (NAG) and N-acetylmuramic acid (NAM). A peptide stem of few amino acids is attached to NAM. The glycosidic bonds between the alternating sugars NAG and NAM form the backbone of the glycan chain [45]. So, if there are on an average m such bonds between adjacent cross-links, then total energy needed to disrupt the chain will be $\approx mE_c$, where E_c denotes the dissociation energy of the bond. Let Σ denote the number of glycan strands crossing per unit area in the fracture plane. We then have

$$G_0 \approx mE_c\Sigma. \tag{7}$$

To relate m to the average length of the glycan chain between adjacent cross-links (say, l_{avg}), we define n to be the average number of glycosidic bonds connecting the disaccharide units between adjacent cross-links [see Fig. 2(b)]. It follows then that $m = 2n$ and $l_{\text{avg}} = (n + 1)$ disaccharides.

We estimate G_0 as follows: the average dissociation energy of a glycosidic bond, specifically, a C-O bond, is of the order of $E_c \approx 6 \times 10^{-19}$ J. The thickness of the cell wall is ≈ 5 nm and the glycan interstrand spacing is ≈ 2 nm (see Table I). We then get $\Sigma \approx (6 \times 10^{16}/\text{m}^2)$. Next we estimate n across a given glycan strand. We have

$$n = \frac{c-1}{i-1}, \tag{8}$$

where c denotes the total number of disaccharide units between the two extreme cross-links in the glycan strand and i denotes the total number of cross-linked peptide stems across the length of the strand. In the limit of long glycan strands spanning the circumference of the cell, we have $n \sim 1/k$, where k denotes the degree of cross-linking across the glycan strand, as is detailed in Appendix D. In the case of *E. coli*, peptide stems rotate around the glycan backbone by roughly 90° per disaccharide [4], so only 50% of the peptide stems are available for cross-linking and it has been observed that the degree of cross-linking is around 30% [28], so $n \sim 3$. However, placing of the cross-links at the terminating units can increase the value of n for shorter length glycan strands substantially. In particular, for glycan strands which are cross-linked at the ends, the value of the numerator in Eq. (8) is maximized. For any glycan strand satisfying this property and allowing for at least two cross-links across the strand, we get $n \sim 3$–6, with strands of length 7–8 disaccharides being optimal in this regard, having $n \sim 5$–6, while in the limit of long glycan strands, we have $n \sim 3$ (see Appendix D for more details). This in particular can explain the following remarkable experimental observations: (1) in Ref. [27], where

HPLC analysis of glycan strand length distribution detected a substantial presence of short length glycan strands, with the length distribution having a mean value of ∼8 disaccharides for about 70% of the strands, and (2) in Refs. [1,28,29], which concluded that $\geqslant 80\%$ of the 1,6 anhydroMur*N*Ac terminal muropeptides are cross-linked and suggested similar proportions of cross-linking at the Glc*N*Ac termini as inferred from peptidoglycan labeled with galactosyl transferase. Our analysis underlines the significance of terminally cross-linked short length glycan strands and in particular, gives an illustration of how design features of the cell wall that underpin the disorder in its structure can affect its mechanical properties in a significant manner.

Glycan strands are initially polymerized in longer lengths of up to 50 disaccharide units and are thereafter shortened by the action of appropriate lytic transglycosylases (LTs), to tailor fit into the PG mesh [46]. Although the exact algorithm that the cell follows to cleave glycan strands is not clear, it is pertinent to note that by appropriate cutting of these strands, the cell can increase the value of n. For instance, n increases when glycan strands are cut in between adjacent in-plane cross-linked peptide stems and interestingly, the preference of glycan strands to maintain terminal cross-links does seem to indicate that LTs which cleave glycan strands subsequent to polymerization, frequently act on them in this manner.

The extent of cross-linking also plays a key role in our analysis. A high degree of cross-linking increases the stiffness of the cell wall [12]. However, it follows from Eq. (7) and Eq. (8) that in this case, the tearing energy is lower, thus making the structure vulnerable to cracks. On the other hand, while a lower degree of cross-linking increases the tearing energy, it also makes the cell wall less stiff [14]. Thus, the extent of cross-linking has to be delicately balanced to ensure optimal levels of stiffness and toughness.

A key mechanism of the cell wall is that of hydrolysis or the cleavage of preexisting peptide and glycosidic bonds in the peptidoglycan mesh. Experiments indicate that *E. coli* mutants which are deficient in hydrolysis enzymes undergo rapid lysis, proving the essential role it plays in ensuring cell viability [47]. Our analysis suggests that peptide bond cleavage due to hydrolysis can secure the cell by increasing resistance to crack propagation: For the crack to propagate, it has to stretch all glycosidic bonds between adjacent cross-links before one of them ruptures. A possible way to arrest the progress of the crack is thus to cleave a peptide bond, so that the number of bonds between adjacent cross-links increases, in other words the value of n increases. This is analogous to the common trick employed by mechanics to arrest the progress of a crack by drilling a small hole at the tip of the crack [48]. The timescale involved in peptide bond cleavage can, however, impose an upper limit on the crack speed, below which bond cleavage action to inhibit crack propagation is feasible—assuming that hydrolases diffuse sufficiently fast to act uniformly across the cell wall and that the mechanical stress on the peptide bonds is only due to the turgor pressure, we first calculate the rate of peptide bond cleavage. In one cell cycle, with time $\tau = 20$ min, a turnover of 40%–50% of the cell wall material takes place [4] and between two adjacent circumferential cross section of the cell, there are ≈ 500 cross-links (with 30% cross-linking and $\sim 2\pi R$ disaccharides comprising all glycan strands in a cross section). So peptide cross-links between two adjacent cross sections are excised at a rate of $k_1 \sim$ 10–12 min^{-1}. Now, since a peptide bond has to be cleaved in the time that the crack front traverses the interstrand distance d, the speed is thus limited to ∼18–24 nm min^{-1} or slower. However, higher stresses on the cross-linkers in the vicinity of the crack tip can potentially lead to a surge in the hydrolytic activity locally. While the exact effect of mechanical stress on the rate of severing of cross-linkers is not clear, it has been hypothesized that increasing stress results in lowering of the energy barrier to hydrolysis, thus resulting in a higher rate of breakage of cross-linkers [3]. Nonetheless, for fast moving cracks, cross-link cleavage is likely to be not fast enough to act. For instance, in the case of *S. aureus*, daughter cell separation, for which mechanical crack propagation has been implicated, happens at speed around 1 μm/s [21]. For crack speed of this order, peptide hydrolysis is unlikely to be able to play a mitigating role.

As we discussed, cross-linked glycan chains in the cell wall ensure that crack propagation in the longitudinal direction is effectively resisted. A natural question then is what is the preferential direction for failure under stress. It has been observed in experiments that rupturing of *E.coli* sacculi tends to occur in the hoop direction, with selective disruption of peptide cross-links between glycan chains [49]. This is particularly intriguing since the bond energies of glycosidic bonds and peptide bonds are very similar [4,49]. A plausible explanation follows from our model: for a longitudinally oriented crack on the cell wall, cross-linked glycan chains crossing the fracture plane have to be taken into account for calculating the tearing energy, as explained above. On the other hand, for a crack aligned in the hoop direction to propagate, only the short peptide cross-links lying in the fracture plane have to be severed. So, the tearing energy in this case is only a fraction of the longitudinal tearing energy, which can lead to a preferential rupturing in the hoop direction. A detailed study of circumferential tears in the cell wall will be carried out in a future work.

Finally, we also mention that here we are neglecting energy dissipation processes as the length of the dissipative zone, which is region around the crack tip where the material is no longer linear elastic and where the bulk of the energy dissipation occurs [9], is very small, ∼5 Å (see Appendix E).

B. Critical crack length

We now calculate critical crack lengths in the planar case as well as the cylindrical case. In Fig. 3 we plot the total energy ($\mathcal{E}_t$), defined as the difference of the strain energy released and the surface energy (see Appendix A), against the crack length, in these two cases, varying the value of n. The critical crack length is obtained at the maxima of the energy curve, which we observe, increases as the value of n increases. For the cylindrical case, the critical crack length is smaller than the planar case, with this difference increasing with increase in value of n. Thus at lower crack length values, the planar case provides a good approximation to the case of a crack on the cell wall under turgor pressure. However, at higher crack lengths, curvature becomes important and the planar approximation starts to break down. In the case $n = 1$, which

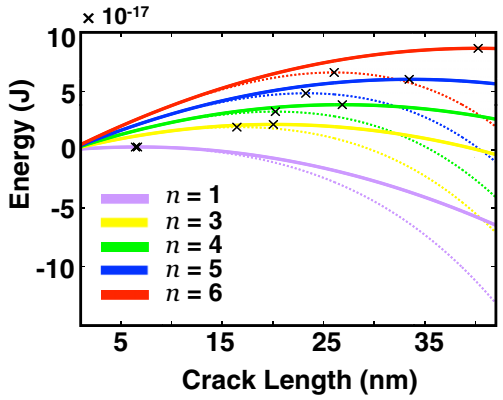

FIG. 3. Total energy $\mathcal{E}_t$ against crack length c, for different degrees of effect of cross-linking. The solid lines represent the plane case, while dotted lines represent the cylinder case. The cross (×) represent the critical crack lengths c_f. For values of the elastic modulus E, the cylinder radius R, and the thickness h, see Table I.

corresponds to a 100% cross-linked sacculi, the critical crack length is small, with $c \approx 6$ nm. When the effect of cross-linking is completely ignored, that is when a very thin crack propagates by disrupting the bonds lying across the fracture plane [so $m = 1$ in Eq. (7)], then critical crack length is even smaller. This underlines the significance of appropriate levels of cross-linking in maintaining the integrity of the cell wall.

Here we use the energy balance criterion to calculate the critical crack length, which is accurately applicable for very thin cracks. For the cell wall, due to the cross-linked structure, the unstrained tip width is approximately the length between two adjacent cross-links, so the length to width ratio in our case will be ∼10–20, which ensures a degree of accuracy. More accurately, this estimate is in fact a lower bound for the critical crack length which well illustrates the reinforcing effect of the cross-linked structure of the cell wall in preventing failure due to cracking (more precise estimates can be obtained by taking the exact geometry into consideration). Interestingly, critical crack total length for the Gram positive bacteria *S. aureus* has been suggested to be around 40 nm [21], which is commensurate to these estimates. Though *S. aureus* has a spherical geometry and its cell wall has a multilayered structure, the composition of the Gram-positive and Gram-negative cell walls remain conserved [50], which suggests that the critical crack length in both cases can be comparable.

A natural question now is whether the role of cross-linking in maintaining the integrity of the cell can be supplanted by other design components of the cell, for instance the cytoskeleton MreB. In the next section, we explore the role of the cytoskeleton in strengthening the cell wall against failure from crack propagation. In particular, we probe if the cytoskeleton can effectively reinforce the cell against crack propagation, even when the effect of cross-linking is discounted.

IV. CYTOSKELETAL REINFORCEMENT

The actin-homologue MreB in bacteria [22,23] is a key component of the bacterial cell. It plays an important role

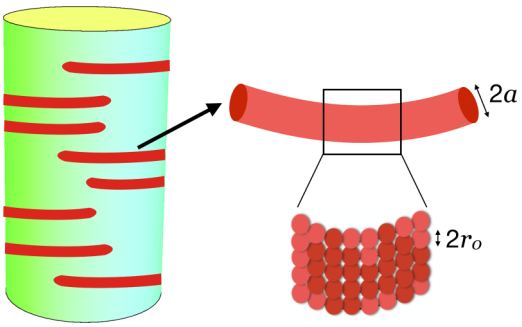

FIG. 4. MreB cytoskeleton modeled as disconnected filament assemblies aligned in the hoop direction, with filament bundle having bundle radius a and preferred radius r. The filament bundle consists of monomers modeled as spheres of radius r_0.

in the growth of the cell and in maintenance of the shape in rod-shaped bacteria [51,52]. In this section, we study the effect of MreB on the toughness of the cell wall, in particular examining the reinforcement of the cell wall by MreB and its effects on the critical crack length.

Several early papers suggested, based on *in vivo* observations, that MreB formed as a cell-spanning helix [23,53]. However, more recent work using high resolution light microscopy have shown that MreB forms disconnected assemblies in the cell that move processively in the hoop direction [54–56] (Fig. 4). Here we model MreB as a collection of disconnected bent cylindrical rods oriented in the hoop direction of the cell.

MreB binds directly to the cytoplasmic side of the inner membrane [57]. While the *in vivo* ultrastructure of MreB is not clear, it has been observed *in vitro* that MreB forms bundles in solutions [58] and binds as filaments to membrane [59]. Biophysical modeling has shown that the orientation of MreB along the direction of maximal curvature is determined by the trade-off between the energetics of filament bending, membrane deformation and the work done against the turgor pressure [60]. For the bacterial cell, the presence of high turgor pressure can ensure that the MreB filaments deform to the cell membrane. In this case, the configuration of MreB is distorted from its preferred shape. *In vitro* studies have shown that MreB filaments are highly curved (with width >200 nm), so the preferred curvature is greater than the typical curvature of the bacterial cell [59]. Therefore, with the preferred radius being smaller than the cell radius, an inward directed pressure is exerted, which we calculate below. It should be noted that for high values of the cross-sectional radius, the energy cost of filament bending increases and it is possible that it becomes energetically favorable for the membrane to deform to the filament [60]. Here, since we are interested in only calculating the inward pressure exerted, we take as an input a configuration of the MreB modeled as bent cylindrical rods of given cross-sectional radius, denoted a, which is deformed from its preferred orientation onto a given orientation determined by the cell radius. We then calculate the pressure exerted for a wide range of values of a, ranging from 3.2 nm [59] to 40 nm [61]. We also note that although MreB has been observed to move persistently around the long axis of the cell over long timescales [54,56], since we are

estimating the average pressure exerted, we will assume that it is localized.

We express the energy functional as an integral over its center line, which is constrained on the cell wall. For such a curve constrained to a surface, given the Darboux frame (see Appendix F for more details), the general energy functional reads [62]

$$\mathcal{E} = \frac{1}{2}\int_0^{L_{\rm fil}} ds[I_{ij}(\kappa_i - c_i)(\kappa_j - c_j) + \beta(\tau - c_t)^2], \quad (9)$$

where κ_i and κ_j are from the set $\{\kappa_g, \kappa_n\}$ of geodesic and normal curvature, and the terms c_i, c_j belong to the set $\{c_g, c_n\}$ of preferred curvatures. The tensor I_{ij} is the inertia tensor. Finally, c_t denotes the preferred twist and β denotes the twist modulus.

We assume that the cross section of MreB complex is circular. The inertia tensor I is thus isotropic and can be written as $I = \alpha\delta_{ij}$, where $\alpha = E_{\rm MreB}\pi a^4/4$, denotes the bending modulus, a denotes the cross section radius and $E_{\rm MreB}$ the elastic modulus. We note that $\beta = \alpha/(1+\nu_m)$ [63], where ν_m denotes the Poisson ratio. We make the simplifying assumption that the Poisson ratio $\nu_m = 0$ for MreB, since this does not qualitatively change our results. So we have $\beta = \alpha$.

Also, it follows from the analysis below that for a wide range of values of the radius a, the elastic energy is several orders of magnitude greater than k_BT, hence we ignore the effect of thermal fluctuations.

A. MreB model

MreB is modeled as several disconnected cylindrical rods, bent and oriented in the hoop direction of the cell, as shown schematically in Fig. 4(b). We will refer to these cylindrical rods as MreB bundles. We assume that the preferred shape of MreB is a bent cylindrical rod, whose centerline can be visualised as an arc of a circle of radius r. In the final configuration, this radius changes to R. Using Eq. (9), together with $\kappa_g = c_g = \tau = c_t = 0$, $\kappa_n = 1/R$ and $c_n = 1/r$, we obtain the total energy for n_f bundles as

$$\mathcal{E}_f = \frac{n_f L_{\rm fil}\alpha}{2}\left(\frac{1}{R} - \frac{1}{r}\right)^2. \quad (10)$$

As we shall see below, the inward pressure exerted by MreB bundles is independent of their length. We thus make the simplifying assumption that the length of all the bundles is the same.

We now estimate the number of MreB bundles of a given radius and length in a typical cell. This depends on the total number of MreB monomers constituting all the MreB bundles in the cell and the number of monomers in a single bundle. We take the volume occupied by the monomers in a single bundle to be in the range $(V_f/2, 3V_f/4)$, where V_f denotes the volume of the bundle. The lower bound of the packing is determined by the substantial elastic modulus of MreB (Table I), which suggests that the monomers will have to be packed reasonably tightly, while the upper bound is determined by the well known Kepler upper bound, given by the recently proved Kepler's conjecture, of ≈ 0.74 [64]. Using this, we estimate the total number of MreB bundles in the cell (Table II) (as detailed in Appendix G).

TABLE II. Range of computed number of disconnected filament bundles in the cell for various observed values of bundle radius and lengths of filament.

	Length		
Radius	250 nm	500 nm	1500 nm
3.2 nm	437–656	218–328	73–109
10 nm	45–67	22–33	7–11
20 nm	11–17	6–9	2–4
40 nm	3–5	1–2	~ 1

The radial force is then given by

$$F_f = \left.\frac{\partial \mathcal{E}_f}{\partial R}\right|_R, \quad (11)$$

and the average pressure exerted is

$$P_f = \frac{n_f L_{\rm fil}\alpha}{2\pi R^3 L}\left(\frac{1}{r} - \frac{1}{R}\right), \quad (12)$$

where L denotes the length of the cylinder. The effective turgor pressure acting on the cell wall is then given by

$$P_{\rm eff} = P - P_f. \quad (13)$$

Experiments have reported shorter length MreB assemblies ($\sim$250 nm) as well as long ones nearly covering half of the cell's circumference ($\sim$1500 nm) [60,61,65]. However, the pressure exerted by MreB is independent of the length of a bundle. This results from fixing the total number of MreB molecules in the cell, which effectively subsumes the role of the length of the bundles (see Appendix G for more details). This also holds when we choose the lengths of bundles to be variable in the cell, present with varying proportions. To illustrate this, we plot the pressure exerted by the MreB against the preferred radius for different values of bundle length and fixed value of bundle radius, taken as 20 nm (left) in Fig. 5. In Fig. 5 (right), we plot the pressure against preferred radius with fixed bundle length taken 250 nm and different values of bundle radius. We observe that for a wide range of preferred radius (0.2–0.4 μm), the pressure exerted even for very large bundle radius is much less than the turgor pressure.

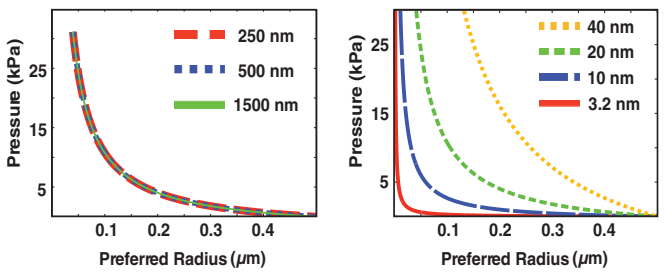

FIG. 5. (Left) Average pressure P_f exerted by MreB vs preferred radius r, for varying filament lengths as given in the inset, with bundle radius fixed at 20 nm. The length independence of the pressure exerted can be observed here. (Right) The pressure exerted against the preferred radius, with fixed bundle length taken 250 nm for different values of bundle radius as in the inset.

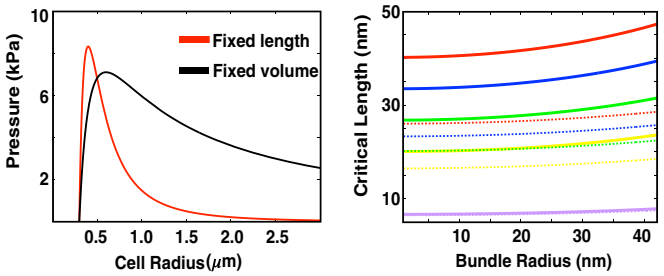

FIG. 6. (Left) Average inward pressure P_f exerted by MreB with preferred radius $r = 0.3$ μm and bundle radius $a = 40$ nm as the radius of the cell R_{cell} varies, in the case length of the cell is fixed (red) and in the case volume of the cell is fixed (black). Note that the pressure exerted in the fixed volume case decays slowly as compared to the fixed length case. (Right) Critical crack length vs Bundle radius for MreB. Lines indicate the planar case, while dotted lines indicate the cylindrical case. In both cases, the degree of effect of cross-linking is taken as indicated, from bottom to top, $n = 1$ and $n = 3, 4, 5, 6$, depending on the length of the glycan strand.

We next explore the variation of the pressure exerted by MreB assemblies as the radius of the cell varies, in particular to understand whether an appropriate change in the dimensions of the cell can result in a significant increase in the pressure exerted by MreB. Fixing h, we plot the pressure exerted against the radius of the cell (Fig. 6, left) in the case that length of the cell L is kept fixed and in the case that volume of the cell $V = \pi R^2 L$, is kept fixed. We infer that as R_{cell} increases, the inward pressure exerted by MreB will become negligible, though as we can deduce from Eq. (12), the decay is much slower in the case when volume is fixed. We observe that interestingly, in both cases, with $r = 0.3$ μm, the pressure exerted attains maxima when $R_{\text{cell}} \approx 0.5$ μm, with similar maxima values, indicating that the pressure exerted will not be significant even if the cell radius is changed. In general, dimensions of the cell may be regulated by a combination of multiple factors, for instance cell width of *Bacillus subtilis* has been suggested to be determined by a delicate balance between the Rod system and class A penicillin binding proteins [66]. In the following, we fix the preferred radius r of MreB to 0.3 μm, noting that our results hold qualitatively over a wide range of values of r (0.2–0.4 μm).

B. Effect on crack length

We now quantify the role of MreB as a determinant of the critical crack length and compare its effect to that of the cross-linked structure of the cell wall. As explained previously, pressure is exerted by MreB in the inward direction. This acts to counter the turgor pressure, resulting in a lowering of the effective pressure on the cell wall. We now examine the effect of this lowering of the pressure, on the critical crack length of the cell wall. We plot the critical crack length against the bundle radius [Fig. 6 (right)]. We take into account the planar case and the cylindrical case, besides incorporating the effect of the cross-linking (with n as in Sec. III A). We note that when the bundle radius is zero, the effect of MreB is negated. So, the critical crack length in this case, is the same as the critical crack length as calculated in the first part, where the effect of MreB was not under consideration. We observe that in all degrees of cross-linking, the critical crack length does not change much even for very large values of bundle radius. This underlines the significance of cross-linking in the protection of the cell wall against cracking.

Recent work has revealed that the outer membrane of *E. coli*, acting in tandem with the cell wall, is the primary mechanical unit of the cell, guarding it against various perturbations [67]. Since MreB, on the other hand, acts on the plasma membrane, this, in conjunction with our analysis, suggests that MreB is unlikely to have a significant direct mechanical contribution in affecting the tearing of the cell wall. It is however possible that MreB indirectly affects the toughness of the cell wall. For instance, a higher concentration of MreB might increase the cross-linking density [12], which can be deleterious for the toughness of the cell wall even as the stiffness of the cell wall will increase.

V. DISCUSSION AND CONCLUSIONS

In this work, we studied the role of the cross-linked structure of the cell wall in ensuring sufficient resistance to crack propagation. We deduced that the tearing energy varies inversely with the degree of cross-linking. We also showed that terminally cross-linked short length glycan strands can dramatically enhance the tearing energy. In particular, we showed that for about 30% cross-linking of the cell wall, as has been observed for *E. coli* [28], the optimal length of the glycan strands for maximizing the tearing energy, are shorter length glycan strands with length ∼7–8 disaccharides, cross-linked at the ends. This provides a possible explanation for surprising experimental observations, which have demonstrated an abundance of shorter length filaments in the peptidoglycan mesh [27] and of the strong preference of glycan strands to cross-link to each other at the termini [28,29]. We estimated the critical crack length for different degrees of cross-linking. Finally, we investigated the effect of MreB reinforcement of the cell wall, modeling MreB as several disconnected bent cylinders and estimated the inward pressure exerted for a wide range of parameters. We concluded that the effect of the cross-linked structure of the cell wall plays the primary role in ensuring the integrity of the cell wall.

In this study, we have computed an average value of the tearing energy G_0 across the sacculus. However, the specific local geometry of the peptidoglycan mesh near the tip of a crack can play an important role in its propagation. Indeed, coarse grained simulations of the peptidoglycan sacculus have indicated the possibility of peptide bonds under stress, like those near the crack tip, ending up aligned even in the circumferential direction [68]. This, for instance, can lead to a local increase in the value of the tearing energy, resulting in higher resistance to propagation of the crack. Detailed numerical simulations are required to delineate the effect of local geometry of the peptidoglycan mesh on the tearing energy, leading upto a more precise calculation of its value and will be undertaken in subsequent work. Nevertheless, since the tearing energy may vary for distinct local geometries near the tip of specific cracks, our study of the average tearing energy across the sacculus assumes significance and paves the way for more exhaustive investigation.

An interesting feature of our analysis is the illustration of a standard dilemma faced when engineering materials, which is to to ensure optimal levels of stiffness and toughness, as the two requirements usually are at cross purposes [8]; in this case, we showed lower degrees of cross-linking result in higher tearing energies, thus offering better protection to the cell wall. On the other hand, a higher degree of cross-linking results in stiffer cell walls [12,14], allowing the cell wall to bear turgor pressure and to preserve its shape. Similarly, longer glycan strands results in enhanced stiffness [26], while shorter length glycan strands can amplify the toughness of the cell wall, as we exhibited. A natural question now is to understand how bacteria maintain an optimal degree of cross-linking, appropriate glycan strand length distribution and precise placing of the cross-links along the strand lengths, fine tuning their structure to ensure the right mix of mechanical properties under a variety of conditions. It will be particularly interesting here to probe the role of hydrolysis, which can affect both the degree of cross-linking and the glycan strand length distribution [15] and which, as we discussed, can mitigate the danger of failure due to crack propagation by cleaving appropriate peptide bridges. Interestingly, treatment of certain strains of *E. coli* with antibiotics like vancomysin [68], which acts by inhibiting formation of new cross-links, often results in bulging of the cell, leading to cell lysis. It has been hypothesised that a build-up of cross-linking defects in a small region under the effect of the antibiotic, leads to formation of a pore in the cell wall, which when it exceeds a critical size, results in irreversible bulging of the plasma membrane through it. Intriguingly, bulge formation does not seem to lead to large-scale cracking of the cell wall, which suggests that the geometry of the pore is such that the critical size for membrane bulging is attained before it becomes energetically favorable for cracking to occur. The precise geometry of such pores formed by the effect of antibiotics is unclear, however under the assumption of a circular pore, a critical pore radius of $\sim$20 nm has been calculated, beyond which irreversible membrane bulging will occur [69]. On the other hand, our calculation indicate critical crack length, denoted c_f, for the cell wall of $\gtrsim$20 nm for axially aligned narrow cracks, it is possible that criticality for membrane bulging is achieved before criticality for large scale cracking, particularly if the pores formed by the effect of antibiotics have a higher radius of curvature at the tips, resulting in lower stress concentrations [42].

The overarching theme of our study was to understand the molecular mechanistic underpinnings of the mechanical properties of the cell wall, in particular its toughness. More experiments are necessary to get a complete understanding of the problem, for instance analogous to those carried out for other biocomposites like nacre, which has an interesting sawtooth-shaped force extension curve, explaining its remarkable toughness [70]. Further, experimental study of the behavior of cracks on the cell wall under varying conditions can elucidate not just the mechanical properties of the cell, but also its growth process, as demostrated in recent experiments using laser nano-ablation, where cuts were introduced on *C. elegans* cell surfaces and were probed to study embryo elongation [38]. An outstanding question in this regard is to probe the self-repair mechanism of the bacterial cell and its ability to heal cracks on the cell wall. Computer simulation, based on the glycan strand length distribution, have indicated the presence of small cracks aligned in the axial direction [16]. Such small cracks, which can play an important role in ensuring passage of nutrients and waste products, can nonetheless develop into critical flaws eventually under the effect of turgor pressure. Hence, these must be regulated by a process of self-repair, a stand out feature of biological systems which is often key to the their remarkable sustainability [71], allowing for design features which are not feasible in human-made structures. Experimentally inducing cuts on the cell wall and studying the healing process will undoubtedly shed more light on this. A plausible method for healing of cracks in this case is that initially, perhaps counterintuitively, peptide cross-links in the vicinity of the crack tip are cleaved by hydrolysis, which as our model explained, can act to locally hike the tearing energy and arrest the progress of the crack. Then wall material is inserted to repair the crack or to apply a mechanical force to close the crack. Since MreB directs peptidoglycan insertion [52], it naturally will play an important role in the crack repair process. In fact, it has been proposed that the observed MreB patch propagation in the circumferential direction is due to stable circumferential propagation of small gaps in the anisotropic sacculus [72]. Our model paves the way for more detailed work, leading up to a precise study of the mechanism by which cracks on the cell surface are healed even as the cell is growing. Such a mechanism will be fundamental to the survival of the cell and an understanding of this will require a comprehensive blend of experimental, computational and theoretical techniques, which can then be leveraged to design new-age antibacterials.

ACKNOWLEDGMENTS

G.R. thanks Satyavani Vemparala for a thorough reading of the manuscript and suggesting several improvements, Gautam I. Menon and Yashodhan Hatwalne for meaningful discussions, and Namrata Gundiah for productive suggestions. I.P. is supported by a DST Inspire Faculty Award (DST/INSPIRE/04/2016/001185).

APPENDIX A: ENERGETICS OF CRACK PROPAGATION

The foundation stone for fracture mechanics was laid by the work of Griffith [36], who studied the energetics of crack propagation. We first consider the case of a centrally placed thin crack of length $2c$ in the infinite plate with uniform thickness h, with the plate represented by the Y-Z plane. The crack is placed on the Z axis, aligned in the Z direction with the middle point of the crack at the origin and a remote load σ applied in the positive and negative Y direction. When an increment in the length of the crack occurs, there is a release of strain energy and crack propagation becomes energetically favorable when this release of strain energy, due to increment in crack length, is greater than the surface energy which is needed to break the bonds of the specimen. The critical point is reached when both are balanced, which we write mathematically as

$$0 = -\frac{d\mathcal{E}_p}{dc} + \frac{d\mathcal{E}_a}{dc} = \frac{d(-\mathcal{E}_p + \mathcal{E}_a)}{dc}. \tag{A1}$$

Here $\mathcal{E}_p$ is the strain energy released, $\mathcal{E}_a$ is the surface energy, dc denotes the crack length increment and we have that the total energy, denoted $\mathcal{E}_t$, is given as $\mathcal{E}_t = -\mathcal{E}_p + \mathcal{E}_a$. So, the critical crack length is the length at which the total energy attains its maxima. It is assumed that the thickness of the material is constant and that the crack growth is slow (quasistatic case). Further, it is assumed that energy dissipation, due to friction and plastic deformations, is negligible.

We note that the strain energy released associated to the crack formation is the same as the work done by the application of a tensile load σ along the crack surfaces in the opening up of the crack. Thus, we have

$$\mathcal{E}_p = 2h\int_{-c}^{c}\frac{1}{2}\sigma u_y\, dz = 2h\sigma\int_{-c}^{c}\frac{1}{2}u_y\, dz. \tag{A2}$$

Here the factor 2 accounts for the two (upper and lower) crack surfaces and u_y denotes the displacement of the upper crack surface, given in the case of plane stress for a thin centrally placed crack as [42]

$$u_y = \frac{2\sigma}{E}\sqrt{c^2 - z^2}. \tag{A3}$$

Substituting this in Eq. (A2) and noting that the rightmost integral simply gives the area of an ellipse with semimajor axis c and semiminor axis $c\sigma/E$, we get

$$\mathcal{E}_p = \frac{\sigma^2}{E}h\pi c^2. \tag{A4}$$

Now, for the crack to propagate, the bonds in the plate have to be broken and hence, an amount of work equal to bond energy must be performed. Let G_0 represent the minimum tearing energy ($\mathrm{J/m^2}$), required for the crack to propagate by breaking bonds in its path. Then, for a crack of length $2c$, we have

$$\mathcal{E}_a = 2G_0 ch. \tag{A5}$$

Substituting $\mathcal{E}_p$ and $\mathcal{E}_a$ in Eq. (A1) appropriately, we get

$$c_f = \frac{G_0 E}{\pi\sigma^2}, \tag{A6}$$

which is the critical crack length, interpreted as the length above which a crack will grow uncontrollably.

APPENDIX B: CRACK ON ORTHOTROPIC CELL WALL

Here we calculate the strain energy released for a crack in orthotropic model of the cell wall and compare it with the isotropic case. For plane stress in the orthotropic case, by Hooke's law, we have

$$\begin{bmatrix}\epsilon_1\\ \epsilon_2\\ \epsilon_{12}\end{bmatrix} = \begin{bmatrix}\frac{1}{E_1} & \frac{-\nu_{21}}{E_2} & 0\\ \frac{-\nu_{12}}{E_1} & \frac{1}{E_2} & 0\\ 0 & 0 & \frac{1}{\mu_{12}}\end{bmatrix}\begin{bmatrix}\sigma_1\\ \sigma_2\\ \sigma_{12}\end{bmatrix}, \tag{B1}$$

where E_1, E_2 denote the elastic modulus, ν_{12}, ν_{21} denote the Poisson's ratio, and μ_{12} denotes the shear modulus.

We consider an infinite orthotropic plate of thickness h placed in the YZ plane, with a crack of length $2c$ placed in the plate, centered at the origin and along the Z axis. Fixing $Z = 1$ and $Y = 2$, we get the strain energy released in this case [73] as

$$\mathcal{E}_{\text{orth}} = \frac{\sigma^2\pi c^2 h}{\sqrt{2E_1E_2}}\sqrt{\left\{\sqrt{\frac{E_1}{E_2}} + \left[\frac{(E_1/\mu_{12} - \nu_{21}E_1/E_2)}{2}\right]\right\}},$$

which we rewrite as [cf. Eq. (A4)]

$$\mathcal{E}_{\text{orth}} = \frac{\sigma^2\pi c^2 h}{\lambda E_0}, \tag{B2}$$

where

$$E_0 = \sqrt{E_1E_2},$$

$$\lambda = \sqrt{2}\left\{\sqrt{\frac{E_1}{E_2}} + \left[\frac{(E_1/\mu_{12} - \nu_{21}E_1/E_2)}{2}\right]\right\}^{-1/2}.$$

In our case, we have $E_1 \approx 25$ MPa, $E_2 \approx 45$ MPa, $\nu_{21} \approx 0.46$, $\nu_{12} \approx 0.2$ [24]. However, the shear modulus μ_{12} of the cell wall is not clear. So, we assume that the cell wall is "specially" orthotropic, which gives $\mu_{12} = \frac{\sqrt{E_1E_2}}{2(1+\sqrt{\nu_{12}\nu_{21}})}$. In this case, we have $\lambda E_0 \approx 36$ MPa, comparable to the value of $E = 30$ MPa that is used to model the cell wall as an isotropic material implying that the strain energy released are quantitatively similar in both cases. So our model framework and the main conclusion of our paper on the role of the cross-linked structure of peptidoglycan mesh in increasing the tearing energy of the cell wall does not change with the inclusion of anisotropy in the model.

APPENDIX C: CURVATURE EFFECT ON STRAIN ENERGY

We now calculate the effect of geometry on the strain energy released due to a through the thickness crack of length $2c$, aligned longitudinally on a pressurized thin cylindrical shell. In this case, apart from in-plane deformations, there is an additional out-of-plane deformation in a small region around the crack resulting from the action of normal force due to internal pressure which is directed through the shell.

The deflection δ in the normal direction, which in this case is the radial direction, varies over the distance l. The bending energy per unit area is given by $e_b \sim \kappa_b\frac{\delta^2}{l^4}$, where we have used that the curvature change is of the order $\frac{\delta}{l^2}$ [63]. The total bending contribution (ignoring all coefficients) concentrated over the area l^2 is then given by

$$\mathcal{E}_b \sim \frac{\kappa_b\delta^2}{l^2}, \tag{C1}$$

where $\kappa_b \approx Eh^3$ is the bending rigidity.

The strain tensor for the stretching energy is of the order of $\frac{\delta}{R}$, that is, $\epsilon \sim \frac{\delta}{R}$, where R is the radius of the cylinder. The corresponding stress is then $\sigma \sim E\frac{\delta}{R}$ and the stretching energy per unit area is given by $e_s = \frac{Eh\delta^2}{R^2}$. Thus, the total stretching energy contribution is (ignoring all coefficients)

$$\mathcal{E}_s \sim \frac{Y\delta^2}{R^2}l^2, \tag{C2}$$

where, $Y = Eh$ is the 2D Young's modulus for the case of plane stress.

The curvature correction energy term $\mathcal{E}_{cyl}$ is therefore given by

$$\mathcal{E}_{\rm cyl} \sim \frac{Eh^3\delta^2}{l^2} + \frac{Eh\delta^2}{R^2}l^2. \tag{C3}$$

Minimizing the total energy in Eq. (C3), $\frac{d\mathcal{E}_{\rm cyl}}{dl} = 0 \Rightarrow l = l_m = \sqrt{Rh}$, which gives us a new elastic length scale for localization of deformation.

Plugging in the value of l_m obtained above, we get

$$\mathcal{E}_{\rm cyl} \sim \frac{Eh^2\delta^2}{R}. \tag{C4}$$

We denote the force acting on the crack periphery, due to internal pressure, by f. Varying $\mathcal{E}_{\rm cyl}$ with respect to δ and equating it to the work done by the force f, we get

$$f \sim \frac{Eh^2\delta}{R}. \tag{C5}$$

The force acts along the line of the crack, and hence, the area over which normal stress is applied is of the order of c^2, where $2c$ is the crack length. It follows then that the force acting is of the order of $f \sim Pc^2$, where P is the internal pressure. Substituting this value of f in Eq. (C5), we get the normal deflection $\delta \sim \frac{Pc^2R}{Eh^2}$. Therefore, using Eq. (C4), we get

$$\mathcal{E}_{\rm cyl} = K_1\frac{Eh^2\delta^2}{R} = K_1\frac{P^2R^2}{Eh}\frac{c^4}{Rh} = K_1\frac{\sigma^2c^2h}{E}\frac{c^2}{Rh}, \tag{C6}$$

where K_1 is a dimensionless constant. This constant $K_1 \sim \pi[0.317\sqrt{12(1-\nu^2)}]$ [39], where ν denotes the Poisson's ratio of the shell material. Since $0 \leqslant \nu \leqslant 1/2$ [24], we have that $K_1 \approx \pi$. Therefore, we get that the total strain energy released is given by

$$\mathcal{E}_i \simeq \mathcal{E}_p + \mathcal{E}_{\rm cyl} = \mathcal{E}_p\left(1 + \frac{c^2}{Rh}\right). \tag{C7}$$

APPENDIX D: GLYCAN STRAND LENGTH AND TEARING ENERGY

In this Appendix, we relate the glycan strand lengths to the tearing energy of the cell wall. Our objective here is to estimate n, the average number of glycosidic bonds connecting disaccharides units between adjacent cross-links, as defined in Sec. III A, which we relate here to the glycan strand length. For any glycan strand denoted g, this value is given by

$$n(g) = \frac{c-1}{i-1}, \tag{D1}$$

where $c(g)$ denotes the total number of disaccharide units between the two extreme cross-links of g (in other words, we are counting those disaccharide units in the glycan strand that lie between any pair of adjacent cross-links) and $i(g)$ denotes the total number of cross-linked peptide stems on the glycan strand g.

We first consider the case when glycan strand lengths span the circumference of the cell wall. In this case, due to periodicity, $c(g) = l(g)$, where $l(g)$ denotes the total number of disaccharide units for glycan strand g. Since l is large, it follows that $n \sim 1/k$ where k denotes the fraction of cross-linked peptides. In the case of *E. coli*, $k \sim 0.3$ [74], so then $n \sim 3$. This also illustrates how a lower degree of cross-linking can enhance the toughness of the cell wall.

However, we now show how smaller length glycan strands cross-linked at the ends, can considerably increase value of n. Let us consider a glycan strand g of length l disaccharide units. It follows from Eq. (D1) that the value of n for a strand of fixed length will be maximized when the peptide stems at the end of the glycan strands are cross-linked. In this case, $c(g) \sim l$. Also, for the degree of cross-linking denoted k, we will have $i \sim kl$. Therefore,

$$n(l) \sim \frac{l-1}{kl-1}. \tag{D2}$$

Taking $k = 0.3$ and allowing for at least two cross-links across the length of the strand, we get $n \sim 3$–6. The value of n decreases as the length of the glycan strand increases and for length of glycan strand $l(g) \sim 7$–8, the value of $n \sim 5$–6. Now, given a glycan strand length distribution p, the average value of n across the cell wall is

$$n_{\rm avg} = \sum n(l)p(l), \tag{D3}$$

where $p(l)$ denotes the proportion of glycan strand lengths of length l. It is clear that a higher proportion of glycan strands of strand lengths ~7–8 disaccharide units will enhance the average value of n across the cell wall. For very short strands with length four disaccharides or fewer, only one peptide stem will be cross-linked with cross-linking degree around 30% [74], so a similar analysis is not possible.

APPENDIX E: DISSIPATIVE ZONE

The length of the dissipative zone, denoted by l_d, is given by

$$l_d = \frac{K_I^2}{2\pi\sigma_t^2}, \tag{E1}$$

where K_I is the stress intensity factor and σ_t is the tensile strength, which is the maximum tensile stress a body can take before failure [42]. We have the strain energy release rate $G = \frac{1}{2h}\frac{d\mathcal{E}_i}{dc}$ and the stress intensity factor is related to the strain energy release rate as [42]

$$G = \frac{K_I^2}{E}. \tag{E2}$$

Now, denoting by Δy_t the maximum stretching of glycan strands, it follows from force balance that

$$\sigma_t = k_g\Delta y_t\Sigma, \tag{E3}$$

where k_g denotes the spring constant of the glycan strands, which is given by

$$k_g = \frac{E}{L_y\Sigma}, \tag{E4}$$

where L_y denotes the length of the glycan strands between adjacent cross-links.

Also, minimum tearing energy, G_0 can be written in terms of k_g as

$$G_0 = \tfrac{1}{2}k_g\Delta y_t^2\Sigma h. \tag{E5}$$

So it now follows from Eqs. (E1)–(E5) that

$$l_d = \frac{L_y}{4\pi}. \tag{E6}$$

Since the typical length of the glycan strand between adjacent cross-links is ~3–6 disaccharides, we have that $l_d \approx 5$Å.

APPENDIX F: CURVES ON SURFACES AND THE DARBOUX FRAME

Let $\mathcal{S} = S(x, y)$ be a surface in $\mathbb{R}^3$. We denote the tangent vectors S_x and S_y, which span the tangent plane to the surface at the $S(x, y)$. Suppose now that we have a curve on the surface, given by the mapping

$$\phi : t \mapsto S(x(t), y(t)).$$

The tangent to the curve at the point $S(x(t), y(t))$ is then given by $\mathcal{T} = x'S_x + y'S_y$. We now define a frame for the curve ϕ (which is thought of as the centerline of the filament bundles under consideration in this work). In this case, we want to use frame to incorporate the information that the curve lies on a surface, thus we will be using the Darboux frame and not the usual Frenet-Serret frame.

Let $\mathcal{T}$ denote the tangent to the curve at $S(x(t), y(t))$ as before. Let $\mathcal{N}$ denote the normal to the surface at $S(x(t), y(t))$. We also further define another unit vector $\mathcal{B}$ as $\mathcal{B} = \mathcal{T} \times \mathcal{N}$. Together, the vectors $(\mathcal{T}, \mathcal{N}, \mathcal{B})$ define the darboux frame for the curve ϕ, lying on the surface $\mathcal{S}$.

It is easy to see, since $\mathcal{T}, \mathcal{N}, \mathcal{B}$ are orthonormal, we have that $\mathcal{T}' \cdot \mathcal{T} = \mathcal{N}' \cdot \mathcal{N} = \mathcal{B}' \cdot \mathcal{B} = 0$ and further

$$(\mathcal{T} \cdot \mathcal{N})' = (\mathcal{B} \cdot \mathcal{N})' = (\mathcal{T} \cdot \mathcal{B})' = 0. \tag{F1}$$

This implies the existence of scalar functions κ_n, κ_g, and τ such that we have

$$\mathcal{T}' = \kappa_n \mathcal{N} + \kappa_g \mathcal{B}, \tag{F2}$$

$$\mathcal{N}' = -\kappa_n \mathcal{T} + \tau \mathcal{B}, \tag{F3}$$

$$\mathcal{B}' = -\kappa_g \mathcal{T} - \tau \mathcal{N}. \tag{F4}$$

Here κ_n is the normal curvature of the curve, κ_g is the geodesic curvature of the curve, and τ is the twist of the curve.

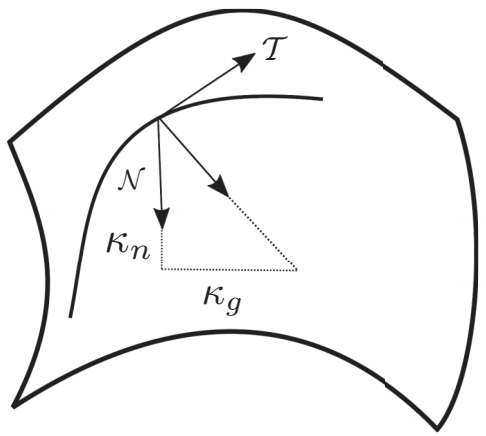

FIG. 7. The Darboux frame describing curves on surfaces, with $\mathcal{T}$ being the tangent to the curve, $\mathcal{N}$ the surface normal. The Darboux frame is $(\mathcal{T}, \mathcal{N}, \mathcal{B})$, where $\mathcal{B} = \mathcal{T} \times \mathcal{N}$.

We can now define the Darboux vector

$$\Omega = \tau \mathcal{T} - \kappa_g \mathcal{N} + \kappa_n \mathcal{B},$$

and thus, we will have

$$\mathcal{T}' = \Omega \times \mathcal{T}, \ \mathcal{N}' = \Omega \times \mathcal{N}, \ \mathcal{B}' = \Omega \times \mathcal{B}. \tag{F5}$$

The Darboux frame for a curve on a surface is illustrated in Fig. 7.

APPENDIX G: MreB FILAMENT BUNDLES IN THE CELL

We estimate the number of MreB filament bundles in a typical cell. The number of MreB monomers has been estimated to lie in the range 17 000–40 000 (see Table I). The number of filament bundles will depend on the number of MreB monomers in a single bundle, which in turn will depend on the radius of the bundle, its length and the packing of the monomers in the bundle. Since the bundle is modeled as a cylinder of length $L_{\text{fil}} = l_f$ and radius a, and monomers are modeled as balls of fixed radius r_0 (see Fig. 4), the number of monomers in the filament bundle will be a fraction of number $n_m \approx \frac{\pi a^2 l_f}{\frac{4}{3}\pi r_0^3}$. This is effectively a problem of packing of balls of uniform radius in a cylinder of given dimensions. It is obvious that not all the volume of the cylinder can be occupied by the balls. Following the resolution of Kepler's conjecture, it is now known that for sufficiently large containers, the volume fraction occupied by balls of a uniform small radius is bounded above by $\frac{\pi}{3\sqrt{2}} \approx 0.74$, which is achieved by cubic close packing or hexagonal close packing [64]. In other words, the densest packings occupy about 0.74 of the volume of the container.

Another possible configuration can be described as follows: we can think of each filament bundle as an aggregation of filaments with each filament having the same number of monomers $\sim l_f/2r_0$. Calculating the number of filaments will thus give us the total number of monomers in this configuration. This is given approximately by dividing the area of cross-sectional circle of the cylindrical container by the area of the equatorial circle of the monomer, giving us the number $\rho_0 = (\frac{a}{r_0})^2$. Here we are assuming that the arrangement is such that the equatorial circles of the monomers on the top cover almost the whole area of the cross-sectional circle of the cylinder and that the monomers are arranged in collection of straight lines, piled below the monomers on the top. Thus, the number of monomers in this arrangement is given by $\frac{l_f \rho_0}{2r_0}$ and it is straightforward to see that in this case, the monomer balls occupy $\sim 2/3$ of the volume of the cylinder.

Now, since the filaments have a robust elastic modulus of around 2 GPa, it is fair to assume to that the packing of the monomers has to be sufficiently dense. On the other hand, since the monomers are much smaller than the cylindrical filament, the upper bound for the volume has to be around 0.74, as explained above. So, we assume that the volume fraction of the monomers in the cylindrical container is ~0.5–0.75. So, with bundle radius denoted a and length denoted l_f, and with total number of MreB monomers denoted N, we have that the number of filaments n_f lies in the range $\frac{28N}{a^2 l_f}$ to $\frac{42N}{a^2 l_f}$,

with a and l_f given in nanometers and where we have used the value $r_0 = 2.5$ nm (Table I). We tabulate (Table II) the number of filament bundles, where the length of such filament bundles taken as 250 nm, 500 nm and 1500 nm, and bundle radius taken as 3.2 nm, 10 nm, 20 nm, and 40 nm. We have assumed here, for simplicity, that all the MreB monomers in the cell are part of some MreB bundle. However, there can be several MreB monomers in the cell cytoplasm, so that the values in Table II give us an upper bound for the number of MreB bundles present in the cell.

[1] W. Vollmer, D. Blanot, and M. A. De Pedro, FEMS Microbiol. Rev. **32**, 149 (2008).
[2] K. D. Young, Annu. Rev. Microbiol. **64**, 223 (2010).
[3] A. Koch, *Bacteria Growth and Form* (Springer, Berlin, 2001).
[4] J. Höltje, Microbiol. Mol. Biol. Rev. **62**, 181 (1998).
[5] S. B. Levy and B. Marshall, Nat. Med. **10**, S122 (2004).
[6] S. J. Lam *et al.*, Nat. Microbiol. **1**, 1 (2016).
[7] J. Gordon, *The New Science of Strong Materials* (Penguin Books, London, 1991).
[8] J. E. Gordon, G. Jeronimidis, and M. O. W. Richardson, Philos. Trans. R. Soc. London A **294**, 545 (1980).
[9] B. Cotterell, *Fracture and Life* (World Scientific, Singapore, 2010).
[10] P.-G. de Gennes and K. Okumura, C. R. Acad. Sci. Ser. IV Phys. **1**, 257 (2000).
[11] J. Keckes *et al.*, Nat. Mater. **2**, 810 (2003).
[12] S. Wang, H. Arellano-Santoyo, P. A. Combs, and J. W. Shaevitz, Proc. Natl. Acad. Sci. USA **107**, 9182 (2010).
[13] Y. Deng, M. Sun, and J. W. Shaevitz, Phys. Rev. Lett. **107**, 158101 (2011).
[14] P. Loskill, P. M. Pereira, P. Jung, M. Bischoff, M. Herrmann, M. G. Pinho, and K. Jacobs, Biophys. J. **107**, 1082 (2014).
[15] R. Wheeler, R. D. Turner, R. G. Bailey, B. Salamaga, S. Mesnage, S. A. S. Mohamad, E. J. Hayhurst, M. Horsburgh, J. K. Hobbs, and S. J. Foster, mBio **6**, e00660 (2015).
[16] D. Pink, J. Moeller, B. Quinn, M. Jericho, and T. Beveridge, J. Bacteriol. **182**, 5925 (2000).
[17] P. Gerhardt and S. H. Black, J. Bacteriol. **82**, 750 (1961).
[18] R. Hughes, P. Thurman, and E. Stokes, Z. Immunitatsforsch. Exp. Klin. Immunol. **149**, 126 (1975).
[19] P. Demchick and A. L. Koch, J. Bacteriol. **178**, 768 (1996).
[20] R. D. Turner, A. F. Hurd, A. Cadby, J. K. Hobbs, and S. J. Foster, Nat. Commun. **4**, 1496 (2013).
[21] X. Zhou, D. K. Halladin, E. R. Rojas, E. F. Koslover, T. K. Lee, K. C. Huang, and J. A. Theriot, Science **348**, 574 (2015).
[22] F. van den Ent, L. A. Amos, and J. Löwe, Nature (London) **413**, 39 (2001).
[23] L. J. Jones, R. Carballido-López, and J. Errington, Cell **104**, 913 (2001).
[24] X. Yao, M. Jericho, D. Pink, and T. Beveridge, J. Bacteriol. **181**, 6865 (1999).
[25] A. Amir, F. Babaeipour, D. B. McIntosh, D. R. Nelson, and S. Jun, Proc. Natl. Acad. Sci. USA **111**, 5778 (2014).
[26] J. C. Gumbart, M. Beeby, G. J. Jensen, and B. Roux, PLoS Comput. Biol. **10**, e1003475 (2014).
[27] H. Harz, K. Burgdorf, and J. V Höltje, Anal. Biochem. **190**, 120 (1990).
[28] M. Schindler, D. Mirelman, and U. Schwarz, Eur. J. Biochem. **71**, 131 (1976).
[29] E. Beachey, W. Keck, M. de Pedro, and U. Schwarz, Eur. J. Biochem. **116**, 355 (1981).
[30] N. Ouzounov, J. P. Nguyen, B. P. Bratton, D. Jacobowitz, Z. Gitai, and J. W. Shaevitz, Biophys. J. **111**, 1035 (2016).
[31] J. J. Thwaites and N. H. Mendelson, Adv. Microbial Physiol. **32**, 173 (1991).
[32] T. Kruse, J. M. Jensen, A. L. Olesen, and K. Gerdes, EMBO J. **22**, 5283 (2003).
[33] H. Kojima, A. Ishijima, and T. Yanagida, Proc. Natl. Acad. Sci. USA **91**, 12962 (1994).
[34] B. Audoly and Y. Pomeau, *Elasticity and Geometry* (Oxford University Press, Oxford, 2010).
[35] M. Levi, *Classical Mechanics with Calculus of Variations and Optimal Control: An Intuitive Introduction* (American Mathematical Society, Providence, RI, 2014).
[36] A. A. Griffith, Philos. Trans. R. Soc. London A **221**, 163 (1921).
[37] A. Boulbitch, B. Quinn, and D. Pink, Phys. Rev. Lett. **85**, 5246 (2000).
[38] T. T. K. Vuong-Brender, M. Ben Amar, J. Pontabry, and M. Labouesse, eLife **6**, e23866 (2017).
[39] E. S. Folias, Int. J. Fract. Mech. **1**, 104 (1965).
[40] F. Erdogan and J. J. Kibler, Int. J. Fract. Mech. **5**, 229 (1969).
[41] L. G. Copley and J. L. Sanders, Int. J. Fract. Mech. **5**, 117 (1969).
[42] R. Sanford, *Principles of Fracture Mechanics* (Pearson, Upper Saddle River, NJ, 2003).
[43] G. Lake and A. Thomas, Proc. R. Soc. London A **300**, 108 (1967).
[44] A. N. Gent and R. H. Tobias, J. Polym. Sci., Polym. Phys. Ed. **20**, 2051 (1982).
[45] M. Bhattacharjee, *Chemistry of Antibiotics and Related Drugs* (Springer, Cham, 2016).
[46] B. Glauner and J. V. Höltje, J. Biol. Chem. **265**, 18988 (1990).
[47] S. K. Singh, L. SaiSree, R. N. Amrutha, and M. Reddy, Mol. Microbiol. **86**, 1036 (2012).
[48] J. Fineberg and M. Marder, Phys. Rep. **313**, 1 (1999).
[49] R. W. Verwer, E. H. Beachey, W. Keck, A. M. Stoub, and J. E. Poldermans, J. Bacteriol. **141**, 327 (1980).
[50] M. Beeby, J. C. Gumbart, B. Roux, and G. J. Jensen, Mol. Microbiol. **88**, 664 (2013).
[51] C. L. White and J. W. Gober, Trends Microbiol. **20**, 74 (2012).
[52] H. Shi, B. P. Bratton, Z. Gitai, and K. C. Huang, Cell **172**, 1294 (2018).
[53] Y. Shih, I. Kawagishi, and L. Rothfield, Mol. Microbiol. **58**, 917 (2005).
[54] E. C. Garner, R. Bernard, W. Wang, X. Zhuang, D. Z. Rudner, and T. Mitchison, Science **333**, 222 (2011).
[55] J. Domínguez-Escobar, A. Chastanet, A. H. Crevenna, V. Fromion, R. Wedlich-Söldner, and R. Carballido-López, Science **333**, 225 (2011).
[56] S. van Teeffelen, S. Wang, L. Furchtgott, K. C. Huang, N. S. Wingreen, J. W. Shaevitz, and Z. Gitai, Proc. Natl. Acad. Sci. USA **108**, 15822 (2011).

[57] J. Salje, F. van den Ent, P. de Boer, and J. Löwe, Mol. Cell **43**, 478 (2011).
[58] P. Nurse and K. J. Marians, J. Biol. Chem. **288**, 3469 (2012).
[59] F. van den Ent, T. Izoré, T. A. Bharat, C. M. Johnson, and J. Löwe, eLife **3**, e02634 (2014).
[60] S. Hussain, C. N. Wivagg, P. Szwedziak, F. Wong, K. Schaefer, T. Izoré, L. D. Renner, M. J. Holmes, Y. Sun, A. W. Bisson-Filho, S. Walker, A. Amir, J. Löwe, and E. C. Garner, eLife **7**, e32471 (2018).
[61] C. Reimold, H. J. D. Soufo, F. Dempwolff, P. L. Graumann, and T. D. Pollard, Mol. Biol. Cell **24**, 2340 (2013).
[62] J. Guven, D. M. Valencia, and P. V. Montejo, J. Phys. A **47**, 355201 (2014).
[63] L. D. Landau, L. P. Pitaevskii, A. M. Kosevich, and E. M. Lifshitz, *Theory of Elasticity, Course of Theoretical Physics*, Vol. 7, 3rd ed. (Butterworth-Heinemann, 1986).
[64] T. Hales *et al.*, Forum Math. Pi **5**, e2 (2017).
[65] S. H. Ye-Jin Eun, Mrinal Kapoor, and E. C. Garner, J. Biol. Chem. **290**, 17181 (2015).
[66] M. F. Dion, M. Kapoor, Y. Sun, S. Wilson, J. Ryan, A. Vigouroux, S. van Teeffelen, R. Oldenbourg, and E. C. Garner, Nat. Microbiol. **4**, 1294 (2019).
[67] E. R. Rojas, G. Billings, P. D. Odermatt, G. K. Auer, L. Zhu, A. Miguel, F. Chang, D. B. Weibel, J. A. Theriot, and K. C. Huang, Nature (London) **559**, 617 (2018).
[68] K. C. Huang, R. Mukhopadhyay, B. Wen, Z. Gitai, and N. S. Wingreen, Proc. Natl. Acad. Sci. U. S. A. **105**, 19282 (2008).
[69] K. E. Daly, K. C. Huang, N. S. Wingreen, and R. Mukhopadhyay, Phys. Rev. E **83**, 041922 (2011).
[70] B. L. Smith, T. E. Schäffer, M. Viani, J. B. Thompson, N. A. Frederick, J. Kindt, A. Belcher, G. D. Stucky, D. E. Morse, and P. K. Hansma, Nature (London) **399**, 761 (1999).
[71] D. Taylor, J. G. Hazenberg, and T. C. Lee, Nat. Mater. **6**, 263 (2007).
[72] S. Taneja, B. A. Levitan, and A. D. Rutenberg, Phys. Rev. E **89**, 012704 (2014).
[73] G. C. Sih, P. C. Paris, and G. R. Irwin, Int. J. Fract. Mech. **1**, 189 (1965).
[74] M. A. de Pedro and F. Cava, Frontiers Microbiol. **6**, 449 (2015).